AD-A045 020 KEO CONSULTANTS NEWTON MA F/G 4/1
IMAGING ALL-SKY PHOTOMETER SYSTEM.(U)
JUN 77 R H EATHER F19628-76-C-0168
UNCLASSIFIED KEO-07 AFGL-TR-77-0155 NL

1 OF 1
AD
A045 020

END
DATE FILMED
11-77
DDC

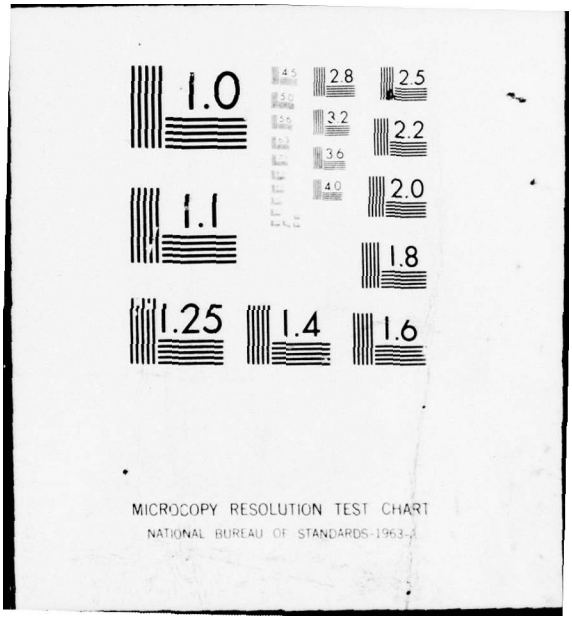
1.0
1.1
1.25
1.4
1.6
1.8
2.0
2.2
2.5
2.8
3.2
3.6
4.0
MICROCOPY RESOLUTION TEST CHART
NATIONAL BUREAU OF STANDARDS-1963-A

AFGL-TR-77-0155

12

IMAGING ALL-SKY PHOTOMETER SYSTEM

Robert H. Eather
KEO Consultants
26 Prentice Road
Newton, Mass. 02159

Final Report
4 March 1976 through 30 June 1977

This research was supported by the Air Force In-House Laboratory Independent Research Fund.

AIR FORCE GEOPHYSICS LABORATORY
AIR FORCE SYSTEMS COMMAND
UNITED STATES AIR FORCE
HANSCOM AFB, MASSACHUSETTS 01731

Unclassified

SECURITY CLASSIFICATION OF THIS PAGE (When Data Entered)

REPORT DOCUMENTATION PAGE		READ INSTRUCTIONS BEFORE COMPLETING FORM
1. REPORT NUMBER AFGL-TR-77-0155	2. GOVT ACCESSION NO.	3. RECIPIENT'S CATALOG NUMBER
4. TITLE (and Subtitle) IMAGING ALL-SKY PHOTOMETER SYSTEM		5. TYPE OF REPORT & PERIOD COVERED Final Report 3/4/76 - 6/30/77 6. PERFORMING ORG. REPORT NUMBER KEO-07
7. AUTHOR(s) Robert H. Eather		8. CONTRACT OR GRANT NUMBER(s) F19628-76-C-0168
9. PERFORMING ORGANIZATION NAME AND ADDRESS KEO CONSULTANTS 26 Prentice Road Newton, Massachusetts 02159		10. PROGRAM ELEMENT, PROJECT, TASK AREA & WORK UNIT NUMBERS 61101 F ILIR 6A01
11. CONTROLLING OFFICE NAME AND ADDRESS Air Force Geophysics Lab. Hanscom AFB, Massachusetts 01731 Monitor/Edward J. Weber/PH		12. REPORT DATE June 30, 1977 13. NUMBER OF PAGES 38
14. MONITORING AGENCY NAME & ADDRESS (if different from Controlling Office)		15. SECURITY CLASS (of this report) Unclassified 15a. DECLASSIFICATION DOWNGRADING SCHEDULE

16. DISTRIBUTION STATEMENT (of this Report)

Approved for public release. Distribution unlimited.

17. DISTRIBUTION STATEMENT (of the abstract entered in Block 20, if different from Report)

18. SUPPLEMENTARY NOTES

This research was supported by the Air Force In-House Laboratory Independent Research Fund.

19. KEY WORDS (Continue on reverse side if necessary and identify by block number)

Imaging photometer, TV system

20. ABSTRACT (Continue on reverse side if necessary and identify by block number)

This report describes the design, fabrication, and demonstration of an all-sky photometric imaging system for narrow-bandwidth auroral and airglow measurements. Testing and use on board the AF NKC 135 research aircraft is described. Reduction and analysis of data obtained on three research expeditions is summarized, and scientific results presented.

DD FORM 1 JAN 73 1473 EDITION OF 1 NOV 65 IS OBSOLETE

Unclassified

SECURITY CLASSIFICATION OF THIS PAGE (When Data Entered)

Summary

An All-sky photometric imaging system was designed and constructed for use on the NKC 135 research aircraft. The system uses film and video recording, and is capable of imaging a 155° field-of-view through four selectable 30 Å filters, and record images of intensity $\gtrsim$ 20 Rayleighs.

The instrument operated successfully and to all specifications on board the aircraft, and supplies a unique new capability to complement the instruments on the plane.

Imaging of various spectral emissions from the aurora allows the determination of fluxes of protons and electrons precipitating into the atmosphere within the field-of-view, as well as average electron energy. System sensitivity allows recording of airglow structure and dynamics. New scientific results have already been obtained as a result of research flights using this instrument.

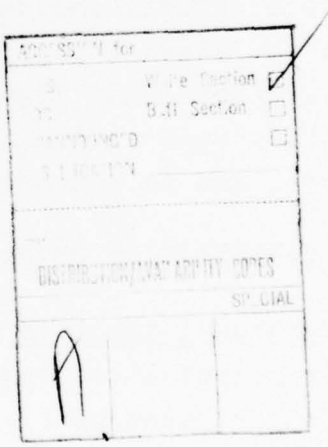

1. INTRODUCTION

The concept of an all-sky photometric imaging device arose from many years of spectrophotometry of the aurora and airglow with traditional photometers. Increased understanding of excitation processes led to the situation where ground-based measurements of auroral spectral intensities and ratios could be confidently interpreted in terms of the parameters of the precipitating particles, i.e., type, flux, and average energy; similarly, increased theoretical understanding of airglow allows interpretation in terms of the dynamics of ionization layers in the E and F regions. But traditional photometric measurements only give information in a given direction at a given time. The next logical advance was to develop a wider field-of-view imaging system that would allow simultaneous determination of these particle parameters over the complete field.

AFGL required such a system to be designed and developed for use on board the NKC 135 research aircraft. The object of procuring such a system was to allow the determination of ionospheric energy input sources, and to monitor the dynamical behavior of the ionization regions so produced. Such measurements have applications to communications (both ground-to-ground and ground-to-satellite) and to ionospheric, auroral, and space physics.

This final report summarizes the design, fabrication, and testing of such a device, and the initial scientific results obtained. Figure 1a. shows a photograph of the mechanical/optics assembly and TV camera head, and Figure 1b. shows the electronic rack assembly. The optics head is mounted to look out a small dome in the top of the aircraft, and is connected to the contraol racks located nearby.

2. RECAPITULATION OF PROGRESS REPORTS KEO-01 → KEO-06

2.1 Personnel involved in this contract:

Principal Investigator:	Dr. R. H. Eather, KEO Consultants
Senior Consultant:	Dr. S. B. Mende, Lockheed Research Labs
Senior Engineer:	Mr. E. Aamodt

2.2 Major subcontracts:

Lockheed Palo Alto Research Labs:	For consulting services of Dr. Mende

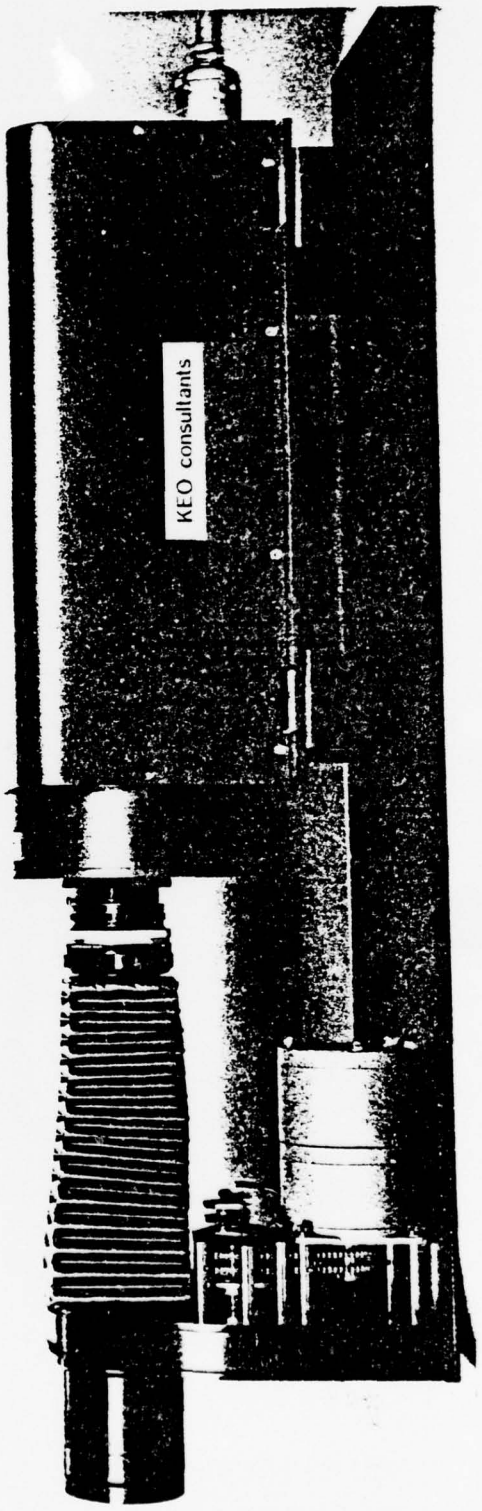

Figure 1a. Mechanical/optics assembly and TV camera head.

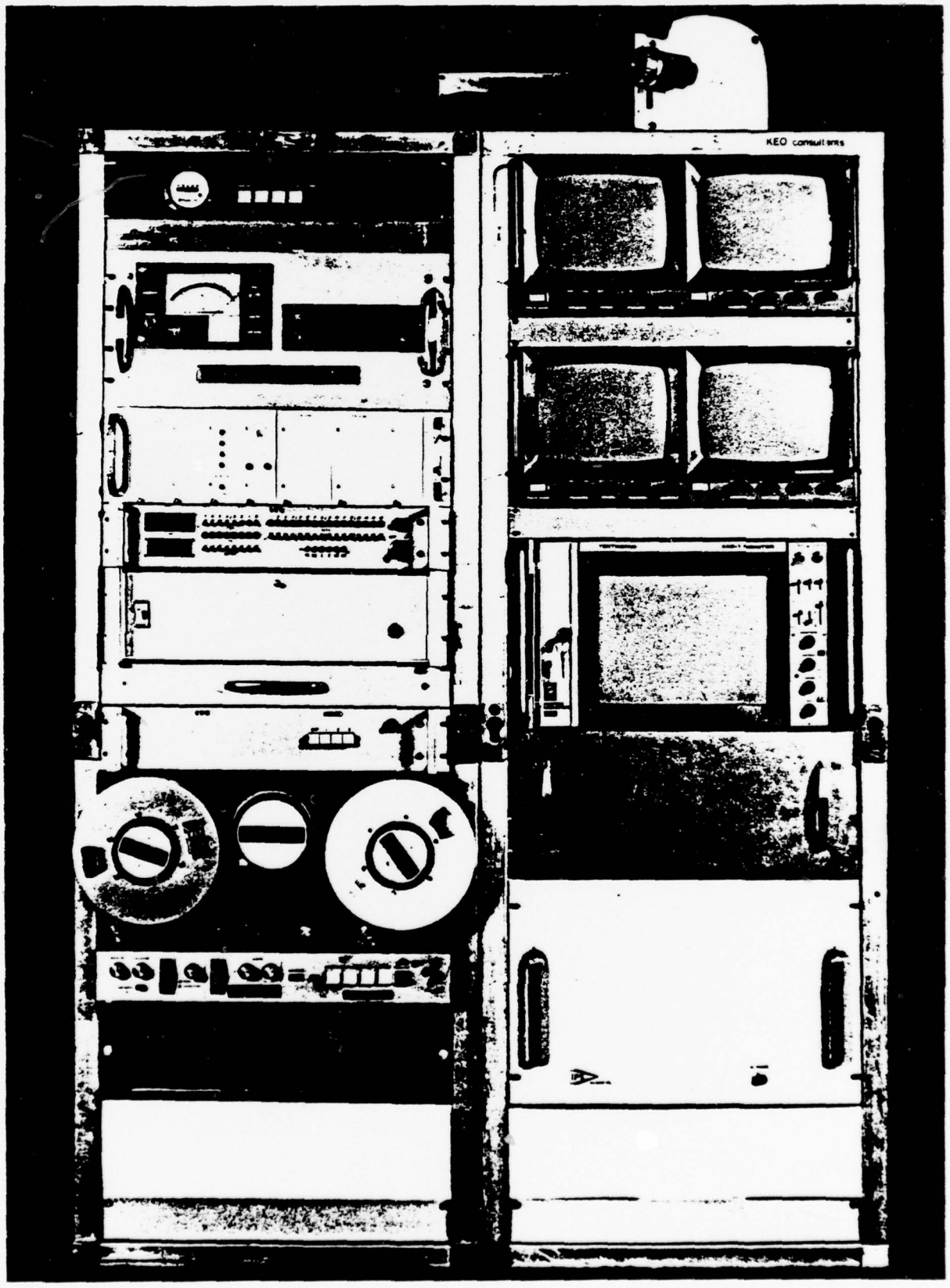

Figure 1b. Electronic control and recording racks.

Systems Management Associates: Fabrication of special-purpose electronics.

Westinghouse: Fabrication of intensified SEC TV camera system.

2.3 Progress each Quarter:

Quarter Ending	Description of Progress
May 31, 1976	Block diagram schematic finalized. Detailed circuit design commenced. Major commercial items selected. Optical system designed and tested with similar components. Optics components ordered. Mechanical-optics system designed and construction commenced.
Aug. 31, 1976	Design Evaluation Report completed and submitted. Detailed circuit design completed and fabrication under way. Completion of optics testing. Mechanical-optics system construction completed. Intensified TV camera accepted from Westinghouse after acceptance testing.
Nov. 30, 1976	All mechanical, electrical and optics fabrication completed and tested. System assembled and tested, and observed by AFGL engineers. System met all specifications, and delivery accepted by AFGL. Draft of Operations Manual complete.
Feb. 28, 1977	Instrument installed on NKC 135 aircraft. Flight tests performed and problems encountered were taken care of. Operating Manual completed. First experimental flights to dayside auroral zone (out of Alaska).

May 31, 1977	Experimental flights north of Goose Bay for co-ordinated experiments with backscatter radar.
	Experimental flights out of Lima, Peru to investigate equatorial airglow structure and relation to radio scintillations and radar reflections.
	Initial analysis of data.
June 30, 1977	Completion of scientific paper on equatorial results.
	Analysis of data from Goose Bay flights still in progress.
	Preparation of final report.

3. DESCRIPTION OF THE ALL-SKY PHOTOMETRIC IMAGING SYSTEM

A primary purpose of the instrument is the real-time monitoring of the major energy influx into the high latitude ionosphere. The instrument uses remote optical sensing by wide-angle, narrow-bandwidth imaging at low light levels. From such information it is possible to derive the type (proton or electron), flux, and average energy of precipitating auroral particles.

Optical remote sensing has the important advantage of providing a continuous description of the precipitating fluxes over a large region of space, so that real-time maps of the precipitating fluxes of both protons and electrons, as well as of average electron energy, can be routinely obtained. Maps of the ionization source function can then be generated over large areas. This instrument presents real-time visual displays of these maps, and greatly enhances the operational flexibility of experimental missions.

A second important application is the monitoring of the development and dynamics of airglow layers. Such changes relate to ionization densities and layer heights in the ionosphere, and may relate to the development of ionization irregularities which affect radio communications.

The system uses a wide angle telecentric optics, narrow band interference filters, and a low light level integrating TV camera to produce video signals from the faint monochromatic auroral and airglow images.

A multi-head video disc is used as a temporary picture storage for the real-time data display of the difference between any two pictures, or the simultaneous color representation of any two pictures on a color TV monitor.

3.1 Summary of system specifications:

Field of view:	150° minimum
Pass Band:	25 Å at f 1.4, 5 Å at f 8
Resolution:	better than 1° in the zenith
Spectral Response:	S-20, exceeding 100 μA/lumen
Picture Storage:	No detectable degradation for up to 3 seconds.
Tube Gain:	Photon noise granularity visible above tube noise.
Temporary Storage:	Video disc, 3 video tracks + 1 sync track.
Permanent Storage:	Video tape deck, time-lapse type (9 hrs. recording time on a single reel): 16 mm color movies camera.
Process Controller:	In-field programming capability.
Display Systems:	4 black and white monitors, 9" diagonal; Color monitor, RGB and A-B input, 12" diagonal.
Real-time Display:	Simultaneous fully registered display of 3 filter channels. Capability of displaying difference of any 2 pictures. Display of 2 or 3 filters as pseudo-color on RGB monitor.
Character Generators:	Date/time display on each frame for frame identification.
Digital Encoding:	Digital encoding of time and housekeeping data for computer controlled data handling.
Flight Heading:	Digital display of flight heading for recording (3 digit BCD TTL compatible

input provided from navigation controls).

Standard Light Source: Built in secondary calibration standard.

3.2 General Functional Description:

To monitor appropriate ionospheric energy input parameters, four relevant wavebands are chosen. The total energy flux of precipitating particles is monitored by recording the 4278 N_2^+ emission band, which is also proportional to the height-integrated ionization rate. The 6300 OI emission is used to obtain the fraction of the total input energy deposited at F-layer height. Considerable energy is deposited and ionization generated by proton precipitation, which is monitored by observation of the 4861 H_β emission. Because H_β is a low-intensity emission, unambiguous interpretation requires knowledge of the nearby background continuum. A control filter is used at 4890 Å to obtain a background picture to subtract from the H_β picture.

A block diagram, Figure 2, shows the components of the system.

A specially-designed telecentric optical system is used to image a 150° field-of-view so that the angle of the ray bundle from each point in the sky is the same and minimal. This maximum ray angle at the filter is 7° of f 1.4, and allows narrow-band (25 Å) interference filters to be used. Even narrower-band filters ($\sim$ 5 Å) could be used if desired, but at the expense of lens speed. For example, the system could be operated at f 8 with a maximum ray angle of 1 1/2°, which would allow the use of $\lesssim$ 5 Å interference filters.

Four filters are mounted on a filter wheel driven by a Geneva mechanism to facilitate rapid interchange of filters (< 0.5 sec). An a.c. synchronous motor drives the Geneva mechanism, which is controlled by a solid state relay and appropriate filter control logic.

Image detection is by two stages of image intensification followed by a SEC TV camera. The TV camera is operated so that the beam is cut off for the duration of the integration period, in which time the picture exposes on the TV tube target and a

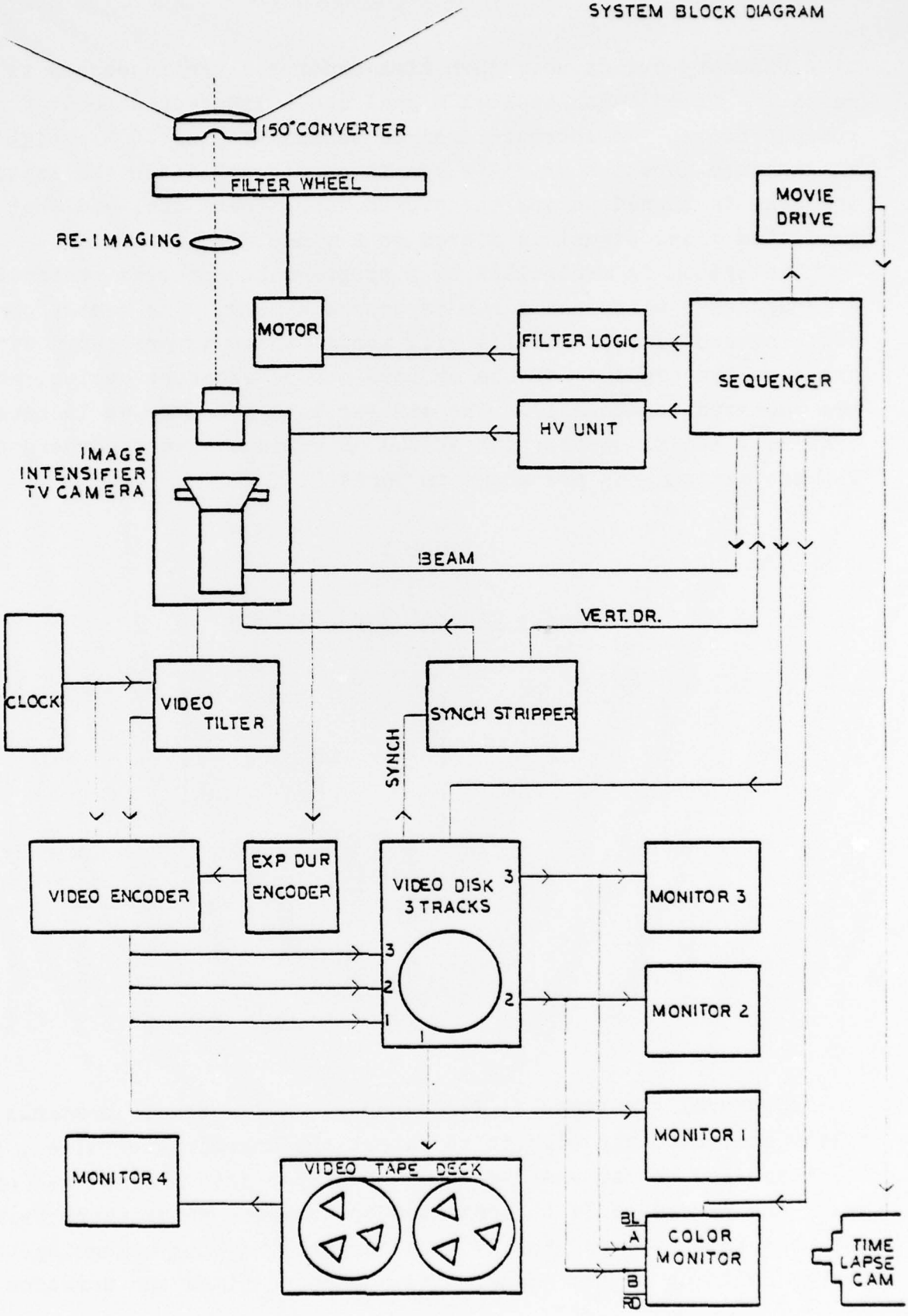

Figure 2: System Block Diagram

time exposure builds up. Such time exposures are necessary to raise the often faint optical signal above inherent camera readout noise. To approach desired sensitivity of 20 Rayleighs, an exposure duration of 1 - 2 sec is required. After the exposure, the beam is turned on and the stored charge read out, and the generated video signal is stored on a video disc.

The system is controlled by a programmable process controller ("sequencer") which has a random access memory. The memory consists of two sets of 256 (16 bit) words, which is preloaded with the complete sequence of one or more chosen exposure cycles, which are repeated continually. The sixteen bits are used as 16 separate control lines to specify the status of various system components. The bit assignments are shown in Table 1.

Table 1

16-Bit Control Word Pattern

1	2	3	4	5	6	7	8	9	10	11	12	13	14	15	16
	GP 1				GP 2				GP 3				GP 4		
Disc 1	Disc 2	Disc 3	Not Used	Beam On-Off	HV 1	HV 2	HV 3	Filter FW1	Filter FW2	Not Used	RGB-Monochrome	Movie Sequence 1	Movie Sequence 2	Movie Sequence 3	Not Used

In auroral experiments, for example, the sequencer commands the filter control logic circuit to select the appropriate filter, and the motorized filter wheel moves this filter into the optical path. Next, the camera would be commanded to commence an exposure by preventing the beam from reaching the TV tube target, and thus beginning the charge build up of the image. The sequencer times the duration

of this first exposure, then commands the video disc to record a frame on one of the tracks. In the following TV frame, the beam is turned on by command and the generated video signal recorded on the disc. In the next TV frame, this picture will be displayed on a black and white TV monitor and is then continually refreshed from the disc. The time-lapse video recorder records the output of one of the disc tracks. The entire process is repeated until all four filters are exposed and the tracks are filled with appropriate picture information and then the cycle repeats. Total cycle time depends on auroral conditions but would typically be 10 - 20 seconds.

To display the difference picture between the H_β image and nearby background image, the difference picture is produced by the video output of disc Track 1 (H_β) and Track 2 (background). This is accomplished by programming the color monitor into the A-B subtraction mode. Since Track 1 is connected to the A input and Track 2 is connected to the B input, the resultant monochromatic picture will be the difference between the two tracks. (In order to maintain perfect registration during the entire sequence of TV frames, the TV camera is synchronized to the fourth (synch) track of the video disc.) This difference signal can be recorded by filming the monitor with the time lapse movie camera.

The system can be used to display two filters, say the 4278 N_2^+ and the 6300 OI, as superimposed color components. If the color monitor is programmed into the color (RGB) mode, such a color composite will be generated. This is because the 4278 N_2^+ signal is recorded on Track 1 which is permanently connected to drive the blue gun of the color monitor and the 6300 OI signal, recorded on Track 2, drives the red gun. The superimposed picture on the RGB color monitor provides a map which can be interpreted in terms of average energy of precipitation across the sky. Permanent record can be made by the time-lapse movie camera.

The third track of video disc is used to generate the permanently updated continuous video for operator supervision and for recording by the video tape deck. This is displayed by one of the black and white video monitors M4 (which is connected to the video output of the tape drive). Thus it serves additionally as

Table 2

Identification of Block Functions in Figure 1

1.	Optical assembly. Wide angle converter, narrow band filters, reimaging lenses, filter wheel, standard light source.	Special-purpose optical-mechanical assembly
2.	TV camera with intensifiers	Modified Westinghouse ETV 6006 Camera
3.	Filter motor drive circuit and logic control.	Special-purpose electronic hardware
4.	HV logic. Controls TV tube gain for each new filter by selecting preset values. Operated by sequencer controller.	Special-purpose electronic hardware
5.	Sequencer	Special-purpose hardware-software
6.	Synch Processor	Special-purpose electronic hardware
7.	Time Clock	Standard hardware ERC Calendar Clock
8.	Digital Video Encoder	Special-purpose electronic hardware
9.	Titler (Video)	Standard electronic hardware 3M Company
10.	Exposure Duration Encoder	Special-purpose electronic hardware
11.	Video Disc. Three video tracks plus sync track	Special-purpose hardware (IPS model disc)
12.	Black and White Monitors for display	Standard hardware (Electrohome 9" monitors)
13.	Color monitor for RGB display	Modified TV hardware (Tektronix 650-1 RGB color monitor)
14.	Time-lapse Tape Recorder	Odetics ITL 700-Modified IVC Video Recorder
15.	Time-lapse Movie Camera	Standard hardware Photosonics 16 mm-1VN Time-lapse Camera

a monitor of the tape drive mod-demod circuitry. M2 is simply a diagnostic monitor showing the instantaneous video as it is coming out of the TV camera.

Housekeeping information is added to the video in two forms. Legible numerals are added by means of a character generator unit (Video Titler). These characters represent heading, Julian date, time (to the nearest 10 seconds), and the position of the filters. The other form of encoding is a set of black and white binary bars which are decodable electronically when replaying the video tape recordings. The encoding is carried out by the Video Encoder Unit. To know the precise duration of the exposure, an exposure duration encoder unit measures the length of the last exposure and provides appropriate code for the video encoder.

3.3 Optics Head Assembly:

The Optics Head Assembly consists of a wide-angle (155°) telecentric lens system (f 1.4) which images the sky onto narrow-band intereference filters. Four such filters are mounted on a filter wheel which is rotated on command by a synchronous motor and a Geneva drive mechanism. Microswitches signal a binary filter-position code.

A C^{14} radioactive light source provides a calibration standard. The intensity may be adjusted according to the narrow-band filter selected, by choice of neutral density filters.

The filter chamber contains a heater and thermostat for temperature control, and temperature is sensed for display by a thermistor.

Narrow-band interference filters were designed so as to optimise spectral selectivity and light gathering power. The filter equation

$$2nd \cos\theta = n\lambda$$

leads to

$$\frac{\delta\lambda}{\lambda} = -\frac{\theta^2}{2n^2}$$

where $\delta\lambda$ is the wavelength shift of peak transmission for angle θ, and n is the effective refractive index of the spacer.

The maximum light cone angle through the filter is 7° at full aperture. It is desirable to select a high index spacer,

so ZnS was specified for the H_β, H_β + 30A and 6300 OI filters. Cryolite had to be used for 4278 N_2^+ as ZnS has low transmission at that wavelength.

Table 3

Center Wavelength	Half Power Bandwidth	Spacer	Wavelength Shift at 7° (Å)
4282	40	Cryolite	14.3
4865	35	ZnS	10.2
4895	35	ZnS	11.6
6307	30	ZnS	13.

All filters are specified to have identical thickness (5/16") so as to maintain focus when filters are interchanged in the image path.

Thermal control is not as stringest as with narrow-band filter systems. However, wavelength shifts of $\sim$ 1 Å/°C will occur, so provision has been made to control filter temperature to within 1° C.

Time taken to change from one filter to the next is 0.4 sec. Minimum time that filter can be in optics path is also 0.4 sec. Minimum time to sequence all four filters is 3.3 sec.

Filter position is indicated by two microswitches in binary notation 0, 1, 2, and 3. Binary 0's are represented by short circuit to ground the binary 1's are represented by open circuit.

A third microswitch ensures that the filters stop in the exact position of the optical train.

The all-sky lens forms an image of the sky in the filter plane (fixed lens system). This image is re-imaged on the face place of the 1st image intensifier by a fixed focus 180 mm focal length lens; followed by Nikon 55 mm f 1.2 lens, with Nikon 3 diopter close-up lens attached. Figure 3 is a schematic of the optics system.

3.4 Sequencer Operation -- Details:

The sequencer is a general programmer unit. It has 16 output (data) lines, each line being assigned by the hardware to a particular control line. The status of the 16 lines as represented by

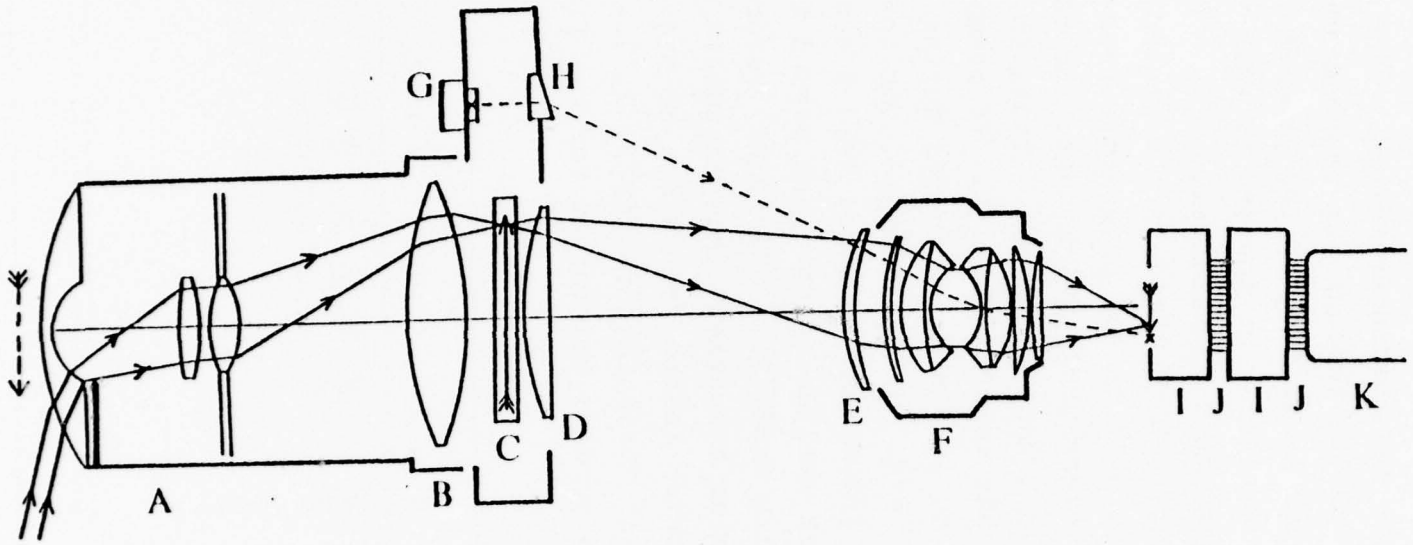

A All Sky Lens (155°)
B 3" F.L. Auxiliary Lens (Bi-Convex)
C Narrow Band Interference Filter
D 7" F.L. Lens (Plano-Convex)
E 3 Diopter Close Up Lens (Meniscus)
F Nikon 55mm/Fl.2 Lens
G Carbon 14 Radioactive Light Source
H Wedge Prism (10 deg.)
I Varo Image Intensifier (Low EBI)
J Fibre Optics Coupling
K Westinghouse LLL SEC TV Tube

OPTICS SCHEMATIC

KEO CONSULTANTS	
SCALE:	APPROVED BY: RHE
DATE: 7/15/76	

Figure 3: Schematic of Optics

16 binary bits is defined as one command word (D_i). A command word is held on the output register for a time which is T_i clock pulses (T_i is an integer). Prior to operation, a sequence of D_i and T_i are programmed into the sequencer memory. During sequencer operation, the sequencer cycles through the preprogrammed sequence. The status of the sequencer is defined by the program counter, PC, which is incremented automatically at the end of each period associated by each preprogrammed T_i interval.

The channel assignment is hard wired in the Control Distribution Unit (CDU). It is a great help to the programmer to have the assignment noted at the top of every programming page, including the condition represented by 1 (i.e., data light on). Thus, in the example below, the first command bit controls Disc 1. If command line is high, i.e., bit is equal to 1, the disc records during that interval. Command line 2 is Disc 2, etc. In the example, for the entry address the PC is zero (PC = 0000|0000) and we would hold the data lines in this position for 60 clock periods (each clock period is a TV field = 1/60 sec). The second data word (PC = 0000|0001) records with Disc 1, all the other bits remaining the same. This status is maintained for two fields = 1 TV frame which is one revolution of the disc. The third word represents: all discs into replay 1, 2, 3 = 0 and beam on (bit 5 = 1). The command word is maintained for two fields.

Step No.	Sequence PC status	Time	1	2	3	4	5	6	7	8	9	10	11	12	13	14	15	16
			Disc 1 Rec.	Disc 2 Rec.	Disc 3 Rec.		Beam	HV 1	HV 2	HV 3	FW 1	FW 2		RGB-M	CAM 1	CAM 2	CAM 3	
0	0000|0000	60	0	0	0		0	1	0	0	0	0		0	0	0	0	
1	0000|0001	2	1	0	0		0	1	0	0	0	0		0	0	0	0	
2	0000|0010	2	0	0	0		1	1	0	0	0	0		0	0	0	0	

4. RESEARCH FLIGHTS

After installation and testing of the all-sky imaging photometer on the aricraft (December, 1976), three research expeditions were carried out using the instrument.

4.1 Dayside Aurora:

During January, 1977 flights were carried out from Fairbanks, Alaska and the U.K., to investigate the dayside auroral region. Subvisual auroral structures in this region were readily recorded, and analysis and interpretation of these data is currently in progress. KEO will participate further in this analysis under a new contract F19628-77-C-0097.

4.2 Nighttime Aurora:

During February, 1977 flights were carried out from Goose Bay, Labrador in conjunction with backscatter radar measurements. The object was for the aircraft to fly under the ionospheric region from which the backscatter occurred, and to use the all-sky imaging system to determine the type of aurora involved. Good data were obtained, and analysis is in progress. KEO will continue to participate under F19628-77-C-0097.

4.3 Equatorial Airglow:

During March, 1977 flights were carried out from Lima, Peru to investigate ionospheric irregularities near the equator that result in radio scintillations of interest to satellite communications. It was shown that these regions are co-incident with airglow depletion regions which were recorded by the all-sky imaging system. This is the first time that a technique has been developed to allow display of the shape and development of the irregularity regions. Future measurements of this type should lead to a better understanding of the time and space morphology of equatorial irregularities, with practical applications to optimizing satellite-to-ground communications.

These results were presented at the American Geophysical Union Meeting in Washington, D.C. on May 30, 1977 by Capt. E. J. Weber. A scientific paper has been written and submitted to the Journal of Geophysical Research, and a copy is attached as Appendix I.

5. CONCLUSIONS

An all-sky imaging photometric system with high sensitivity was designed and developed for use on the NKC 135 research aircraft. The instrument has operated successfully and to all specifications in the airborne environment, and is a valuable addition to the instrument complement on the plane. New scientific results have already been obtained, and it is expected that the instrument will allow several new and relevant ionospheric and auroral experiments over the next few years. The instrument supplies a unique capability to the Ionospheric Dynamics Branch at AFGL, as it is one of only two such instruments in existence. Future investigations will include equatorial airglow structures, and co-ordinated missions that overfly ground meridian chains of photometers and magnetometers in the auroral zone.

Appendix I

North-South Aligned Equatorial Airglow Depletions

E. J. Weber[1]
J. Buchau[1]
R. H. Eather[2]
S. B. Mende[3]

July 1977

[1]Air Force Geophysics Laboratory, Hanscom AFB, MA 01731
[2]Department of Physics, Boston College, Chestnut Hill, MA 02169
[3]Lockheed Palo Alto Research Laboratories, Palo Alto, CA 94304

ABSTRACT

A new instrument for all-sky, spectrophotometric imaging of aurora and airglow has been installed in the Air Force Geophysics Laboratory's Airborne Ionospheric Observatory. Initial observation of equatorial and near-equatorial 6300 Å OI airglow show the existence of north-south aligned regions of airglow depletion. These dark bands often extend more than 1200 km in the north-south direction and 50 to 200 km in the east-west direction. They are observed to drift toward the east during the evening-midnight hours; with one observation of westward drifts after local midnight. Airglow fine structures associated with the boundaries of the dark bands have been observed down to 2.5 km resolution limit of the instrument. Simultaneous airborne ionospheric soundings indicate that these regions of airglow depletion are characterized by an increase in the virtual height of the F-layer. A simple model of field aligned electron density depletion in the bottomside of the F-layer explains both the airglow observations and the ionospheric soundings.

INTRODUCTION

A new instrument for monochromatic, all-sky observations of auroral and airglow emissions has recently been installed in the Air Force Geophysics Laboratory's Airborne Ionospheric Observatory, an NKC-135 aircraft instrumented for ionospheric research. Initial equatorial airglow and F-region irregularity measurements are presented in this report.

The instrument is a wide field-of-view, narrow spectral bandwidth, TV system designed to operate in a time exposure mode. A detailed description of a similar system has been given by Mende and Eather (1976) and Mende et al. (1977).

A series of seven flights were conducted along the west coast of South America in March 1977 to investigate the spatial and temporal characteristics of large scale, F-region irregularities in the vicinity of the magnetic equator. The primary purpose of this expedition was to relate specific dynamical features of the equatorial ionosphere to the occurrence of signal fluctuations (scintillations) on satellite-to-aircraft and satellite-to-ground VHF/UHF radio transmissions. Optical imaging measurements were performed with the objective of identifying large-scale, airglow structures which are associated with the F-region ionospheric (electron density) irregularities. Simple modelling shows that the existence of a bottomside ionization corrugation or depletion colocated with the moving band of airglow depletion can explain the observed ionogram signatures.

EQUATORIAL AIRGLOW STRUCTURES

Departures from spatially uniform airglow emission occur as regular features of the equatorial, and near-equatorial ionosphere. The prominent intertropical arcs (Barbier, 1961; Barbier et al., 1961) appear as two bands of enhanced 6300 Å OI which reach maximum intensity at ± 12° magnetic latitude, and display symmetry with respect to the dip equator. These bands coincide closely in position with the Appleton anomaly region of enhanced F-region electron density. A summary of intertropical arc morphology is presented by Weill (1967), and Kulkarni (1974). Smaller scale airglow

structures have also been investigated. Steiger (1967) presented photometric sky maps of 6300 Å and 5577 Å airglow structure from Haleakala Observatory, Hawaii. These show the existence of localized (∿ 500 km diameter) enhancements in 6300 Å intensity, primarily to the south of the observing station. Less frequently, highly structured north-south aligned ridges or fingers of enhanced 6300 Å emission have been observed. The 6300 Å enhancements are frequently accompanied by similar variations in 5577 Å. Van Zandt and Peterson (1968) have shown that tropical airglow structures at 6300 Å and 5577 Å can take a variety of forms; from east-west aligned bands or arcs to narrow north-south ridges of alternately enhanced and diminished intensity, arranged along an east-west band. Eastward drift velocities on the order of a few hundred km/hr have been reported for some of these airglow irregularities. The ridges shown by van Zandt and Peterson are typically inclined to the west of geographic north, such that at the latitude of Hawaii (∿ 20° magnetic), the structures are not aligned along magnetic field lines.

From simultaneous ionosond measurements, both van Zandt and Peterson (1968) and Steiger (1967) conclude that spatial variations in 6300 Å OI intensity result primarily from variations in the height of the F-region rather than from changes in the electron number density at peak of the F-layer. The gradients in 6300 Å intensity along the east-west direction appear, then, to be the result of corrugations in the bottomside of the F2 layer. The co-variation of 6300 Å and 5577 Å OI, within these airglow enhancements clearly requires an F-region source for 5577 Å OI airglow in addition to the relatively uniform and steady E-region.

OBSERVATIONS

All-sky (155° field-of-view) images of the equatorial airglow were made through 6300 Å and 5577 Å narrow band (∿ 30 Å) interference filters, using alternate 2.5 second exposures to produce an image at each wavelength every thirty seconds. The resulting TV frames were then recorded on video tape and also by photographing the TV monitors.

Figure 1 presents a series of 6300 Å images (photographs of the tape recorded video frames) obtained during a flight on 17 March 1977, at fifteen minute intervals between 0100 and 0545 UT. The superposed grid indicates the

projection of Corrected Geomagnetic (CG) longitudes (or magnetic meridians) at one degree intervals, for an assumed emission height of 250 km. The flight track for 17 March 1977 was a series of north-south legs (from 3° CG North to 3° CG South) along a magnetic meridian 3° west of Lima, Peru. All images have been reoriented with magnetic north on top as shown in Figure 1. (The reversal of east and west is a result of the display scheme used.)

Care must be exercised in the interpretation of features near the edge of the field-of-view. Although the van Rhijn effect tends to increase the apparent airglow intensity at large zenith angles (× 2.7 for 75° zenith angle at 250 km emission height), the wide angle lens suffers serious vignetting toward the edge of the field-of-view (× 3.3, Mende et al., 1977). The two effects act in opposition, but vignetting exceeds van Rhijn enhancement at the edges, often resulting in a perceptable dark band around the image for the weak airglow features under consideration. The narrow N-S striations about 1/2° from zenith that can be seen in most images are the ionosonde antennas which stretch above the all-sky lens. They appear east or west of zenith depending on whether the plane is flying north or south.

The images between 0100 UT and 0200 UT show a low level unstructured glow (∿ 60 R) with some enhancement towards the south, probably enhanced emission from the maximum of the Appleton anomaly. A slight patchiness is evident in the center of the 0130 UT and 0145 UT images. The 0215 UT image shows a prominent depletion in the 6300 Å airglow in form of a dark band which extends south to north along much of the western horizon. The formation of this dark band can be seen as early as 0200 UT. Within the next 2.5 hours this band travels across the sky, leaving the instrumental field-of-view on the eastern horizon by approximately 0445 UT. Generally the images show that the eastern or leading edge of the airglow deplation is closely aligned in the magnetic north/south direction, (best seen in the 0330 UT image). However, inspection of selected images suggests the possibility of a 5° skew (best seen in the 0345 UT image) with the southern end of the edge leading the northern end. A detailed analysis involving the measurement of selected stars is required to eliminate experimental causes (such as small aircraft heading errors) before the precise alignment can be measured. The leading edge displays a sharp intensity gradient in the east-west direction. From absolute airglow intensities, independently measured on the aircraft by a vertically directed, 1 meter Ebert-Fastie

scanning spectrometer, a decrease from 75 R to 15 R within 100 km has been determined (J. G. Moore, private communication, 1977). The western edge of the depletion region shows a somewhat more gradual, structured transition to the adjacent bright airglow region. The width of the depletion when directly overhead at 0330 UT is approximately 150-200 km between 0300 and 0345. The width of the measured depletion region also depends on the detectability threshold of the instrument, so system gain changes can affect the apparent width of these features, but, for the measurements in Figure 1, only small gain changes were necessary. In the north-south direction, these regions extend across the entire field-of-view to include a horizontal distance of more than 1200 km, assuming a 250 km emission height.

The images at 0415 and 0430 UT show the appearance of a second region of airglow depletion drifting into the field-of-view from the west. This second region seems to be "filled in" before reaching the aircraft. Unstructured airglow ($\sim$ 150-200 R) covers (most of) the observable sky until 0515 UT and then rapidly falls in intensity ($\sim$ 100 R), leaving only minor enhancements towards the southern and western horizons.

DRIFTS

The CG Longitude of the eastern and western edges of the airglow depletion, on an east-west great circle through the aircraft zenith, were determined for the feature in Figure 1. The results (Figure 2) indicate that the deplation defited toward CG East with a relatively constant velocity of $\sim$ 90 m/sec, while maintaining an east-west dimension of $\sim$ 165 km. Eastward drfits from 50 to 100 m/sec were observed on other local evening flights. During a flight from Lima, Peru to Homestead AFB, Florida, on 26 March 1977,a clear reversal from eastward to westward drift was observed. This occurred in the midnight (0035 LT) sector with the aircraft located at 16° CG latitude. This was the only observation of westward drifts during the expedition.

IONOSONDE MEASUREMENTS

Figure 3 presents results of the ionospheric soundings conducted simultaneously onboard the aircraft. The virtual height of the observed

F-layer and the virtual range of oblique F-layer echoes is shown as a function of time. The oblique echoes are first observed at a virtual range of 800 km at 0157 UT closely coincident with the time when the depletion is first observed on the western horizon. These oblique returns close in range, consistent with the approach of a reflecting or scattering region, and merge with the overhead F-layer by 0317 UT.

By 0335 UT oblique echoes are seen to separate from the lowest F-region trace and to increase in range to about 350 km by 0345 UT. After this time they are obscured by other returns and cannot be further identified. Even though the omnidirectional sounder antenna does not permit determination of the angle of arrival of the oblique echoes, the coinciding time histories of the airglow depletion movement and the backscatter range change suggest that the sounder observes the motion of ionospheric scattering regions associated with the motion of the depletion. Assuming a height of 250 km for the scattering region, ranges of the approaching backscatter front were converted to ground distances. The estimated locations of these approaching scattering regions are shown as white dots in the respective airglow images in Figure 1, to the west of zenith. Ground ranges derived from the receeding backscatter branch, observed after the overhead passage of the leading edge of the depletion, were entered as black dots to the east of the zenith of the respective images. As Figure 1 shows, best seen in the 0245 to 0315 UT images, the approaching backscatter is tracking the trailing (western) edge of the depletion, while the leading (eastern) edge is tracked by the receeding echoes observed after 0330 UT.

A model of an ionization depletion in the bottomside of the ionosphere shown in Figure 4 produces a sequence of approaching and receeding echo traces as well as a variation in h'F, which closely resemble the observations. With the aircraft located to the east of the structure, returns are received vertically and via ray path b1; after passage of the structure to the east of the aircraft, returns are received vertically and via ray path b2. From the all-sky images the width of the structure has been taken as 165 km, and the velocity as 92 m sec^{-1}. The time of passage of the eastern edge through the aircraft zenith was determined as 0308 UT. The virutal heights of the F-layer prior to and after the passage of the depletion were taken from Figure 3 as 240 km respectively. Figure 4 shows the result of the model computations with the relevant sections of the h'

plot from Figure 3 superimposed.

The fit is generally good but additional strong returns associated with the trailing edge of the depletion at ranges larger than derived from the simple model, and approaching at a greater speed suggest a more complex structure of the trailing edge than modelled. Analysis of the 16 mm photographic record, with thirty second time resolution, shows distinct structure with turbulent motion at the western edge of the depletion, in contrast to the smooth and stable features observed at the eastern edge. The east-west assymmetry is also visible in Figure 1. The 0330 UT image shows diffuse and patchy structure at the trailing edge compared to the well-defined leading edge. These features may be responsible for the more complex ionosonde backscatter associated with the trailing edge. The model used to explain the sonder measurements is a simplification of the bottomside effects of an instability model proposed by Woodman and La Hoz (1976) to describe the development and subsequent upward propagation of bubbles of low electron density in the equatorial F-region. This process explains the time history of irregularity structures of plumes observed by the Jicamarca 50 MHz radar. Comparison of the Woodman and La Hoz model with the model used in the present work suggests that the airglow depletions described here are a manifestation of the same phenomenon leading to the Jicamarca plume observations. The present model also suggests the existence of strong east-west electron density gradients extending over a considerable north-south extent and moving in an eastward direction. These moving fronts are presumably associated with discrete patches of scatters observed through trans-equatorial HF propagation experiments (Röttger, 1973). The distinct difference in structure of the leading and trailing edge of the airglow depletion deduced from the observations of this isolated event may also be responsible for the east-west assymmetry observed in backscatter measurements at 27.8 MHz (Kelleher and Skinner, 1971).

A detailed model of the structure of the F-layer within the airglow depletion cannot be deduced from the available ionograms. The ionogram traces required to establish the Ne (h) profiles are either obscured by the scattered reflections received from the edges of the depletion (see Figure 4) or the traces do not exist due to the irregular structure within the depletion. This limitation of ionosondes to establish profiles within regions of strong horizontal gradients is well known in the high latitude

ionosphere; although the main F-layer trough is clearly identifiable in ionograms, the profiles inside the trough cannot be determined due to the narrowness of the depletion (Lobb and Titheridge, 1977).

After merging of the approaching front with the overhead trace, strong unstructured spread F develops, which persists for the period of passage of the depletion. Throughout the evening, the F-layer had come down, initially from 275 km (0000 UT) to 230 km (0300 UT) just prior to the overhead arrival of the leading edge of the depletion. The layer rapidly moved upwards by 35 km, reaching a maximum h' of 265 km by 0319 UT, the time of strongest spread F. After this, the layer again rapidly moved down to 215 km (0332 UT) and fluctuated around this level for the remainder of the observations. Some close range oblique echoes between 0437 UT and 0500 UT are possibly remnants of the ionospheric disturbance associated with the short-lived depletion observed near the western horizon between 0415 UT and 0430 UT.

foF2 values observed between 0100 and 0500 UT are rather uncertain because of spread conditions and high nighttime HF noise levels, but in general fluctuated between 8.5 and 9.5 MHz. After 0500 UT the spread and noise conditions improved and a clear decrease of the foF2 from 9.2 MHz (0503 UT) to 8.0 MHz (0523 UT) and finally to 5.8 MHz (0549 UT) is observed, which follows the decrease of the overall brightness of the 0500 UT to 0545 UT all-sky photometer images. Since h'F does not change appreciably (from 212 km at 0503 to 226 km at 0549 UT) this change in airglow level is directly attributable to the foF2 decay.

SUMMARY AND DISCUSSION

Monochromatic, all-sky imaging has revealed the existence of north-south (magnetic) aligned regions of airglow depletion in the equatorial F-region. East-west scale sizes of these depletions ranged from 50 to 200 km, with fine structure detectable on the 16 mm photographic records as small as 2.5 km (instrumental resolution at 250 km altitude). Observations during several flights in the immediate vicinity of the magnetic equator in March 1977 show that these depletions drift toward the east with speeds of 50-100 m/sec during the local evening hours. One example of a reversal from eastward drift velocity to westward drift was observed in the midnight (0035 LT) sector, with the aircraft located at 16° CG north. During this expedition, airglow

were regularly observed provided the virtual base height of the adjacent F-layer (h'F) was below 275 km. Base heights in excess of 275 km lead to greatly diminishes airglow intensities, thus precluding observations of ionospheric irregularities by optical techniques.

The interpretation that the 6300 Å decrease inside the observed depletion is the result of the rising of the base height of the nighttime F-layer above the 275 to 300 km level is supported by interpretation of the observed h' and backscatter range variations using a simple bottomside Ne corrugation model.

A bottomside Ne depletion, extending for more than 1200 km in the north-south direction with an east-west width of 100 to 200 km and with a base height of the F-layer around 300 km, colocated and moving with the 6300 Å depletion explains both the observed 6300 Å airglow structure and the ionospheric observations. Because of constraints previously discussed, neither the optical nor the ionosonde techniques allow a determination of the minimum F-layer base height within the region of diminished ionization.

This interpretation is consistent with recent results of McClure et al. (1977) who regularly observe biteouts in the ion density after sunset of up to three orders of magnitude with the Atmospheric Explorer satellite AE-C. These range in altitude from the peak of the F-layer up to $\sim$ 600 km and have typical upward plasma velocities of several tens to several hundreds m/sec. The model used to explain the sounder observations has strong similarities with the response of the bottomside to a bubble model proposed by Woodman and La Hoz (1976). From the similarity of the two phenomena and the models it is reasonable to postulate that airglow depletion are the optical signatures of these biteouts or bubbles. Because of the complementary nature of satellite plasma measurements and airborne imaging photometer measurements, coordinated experiments would provide insight into the initial development of these regions of upward plasma flow. Also, the ability of an airborne observatory to monitor a single region of airglow depletion for several hours would allow successive satellite measurements of ion composition changes during the lifetime of a single bubble.

ACKNOWLEDGEMENTS

The authors wish to thank J. G. Moore for providing the airborn

spectrometer measurements, J. W. F. Lloyd for assistance in operation of the all-sky imaging photometer, and J. P. McClure and A. L. Snyder for helpful comments in the preparation of this paper.

The success of this airborne expedition is due to the efforts of Maj. Calvin Smith and other members of the 4950th Test Wing, Wright Patterson AFB, Ohio.

This research was supported by the Air Force In-House Laboratory Independent Research Fund of the Air Force Geophysics Laboratory, Air Force Systems Command.

REFERENCES

Barbier, D., Les Variations D'Intensite La Raire 6300 Å La Lumenescence Nocturne, Ann. Geophys. 17, 5, 1961.

Barbier, D., G. Weill and J. Glaume, L'Emission de la Raie Rouge der Ciel Nocturen en Afrique, Ann. Geophys. 17, 305, 1961.

Kelleher, R. F. and N. J. Skinner, Studies of F-region irregularities at Nairobi, Ann. Geophys. 27, 195, 1971.

Kulkarni, P.V., Tropical Airglow, Ann. Geophys. 30, 105, 1974.

Lobb, R. J., and J. E. Titheridge, The Effect of Travelling Ionospheric Disturbances on Ionograms, J. Atmos. Terr. Phys. 39, 129, 1977.

McClure, J. P., W. B. Hanson and J. H. Hoffman, Plasma Bubbles and Irregularities in the Equatorial Ionosphere, J. Geophys. Res., in press, 1977.

Mende, S. B. and R. H. Eather, Monochromatic All-Sky Observations and Auroral Precipitation Patterns, J. Geophys. Res. 81, 3771, 1976.

Mende, S. B., R. H. Eather and E. K. Aamodt, Instrument further Monochromatic Observation of All-Sky Auroral Images, Appl. Opt. 16, 1691, 1977.

Röttger, J., Wave-like Structures of large-scale equatorial spread-F irregularities, J. Atmos. Terr. Phys. 35, 1195, 1973.

Steiger, W. R., Low Latitude Observations of Airglow, Aurora and Airglow (B. M. McCormac, ed.) Reinhold Publ. Co., p. 419, 1967.

Van Zandt, T. E. and V. L. Peterson, Detailed Maps of Tropical 6300 Å Nightglow Enhancements and their Implications on the Ionospheric F2 Layer, Ann. Geophys. 24, 747, 1968.

Weill, G. M., Airglow Observations Near the Equator, Aurora and Airglow (B. M. McCormac, ed.) Reinhold Publ. Co., p. 407, 1967.

Woodman, R. F. and C. La Hoz, Radar Observations of F-Region Equatorial Irregularities, J. Geophys. Res. 81, 5447, 1976.

FIGURE CAPTIONS

Figure 1. All-sky (155° field of view) 6300 Å OI airglow images at fifteen minute intervals, from 0100 UT to 0545 UT, 17 March 1977. The superposed grid indicates the projection of C. G. longitudes, at one degree intervals, for an assumed emission height of 250 km. The black and white dots represent respectively the location of approaching and receeding oblique F-region ionosonde backscatter returns.

Figure 2. The C. G. longitude of the eastern and western edges of the airglow depletion shown in Figure 1.

Figure 3. Virtual height/range plot of ionosonde returns associated with the 6300 Å airglow depletion. The shaded areas represent range spread on backscatter returns or overhead spread F conditions.

Figure 4. Model of an eastward drifting, bottomside Ne depletion or corrugation based on observed ionosonde and airglow parameters. The measured ranges of oblique returns and the virtual height of the overhead F-region are compared with range/height changes expected from the passage of the model bottomside structure over the ionosonde.

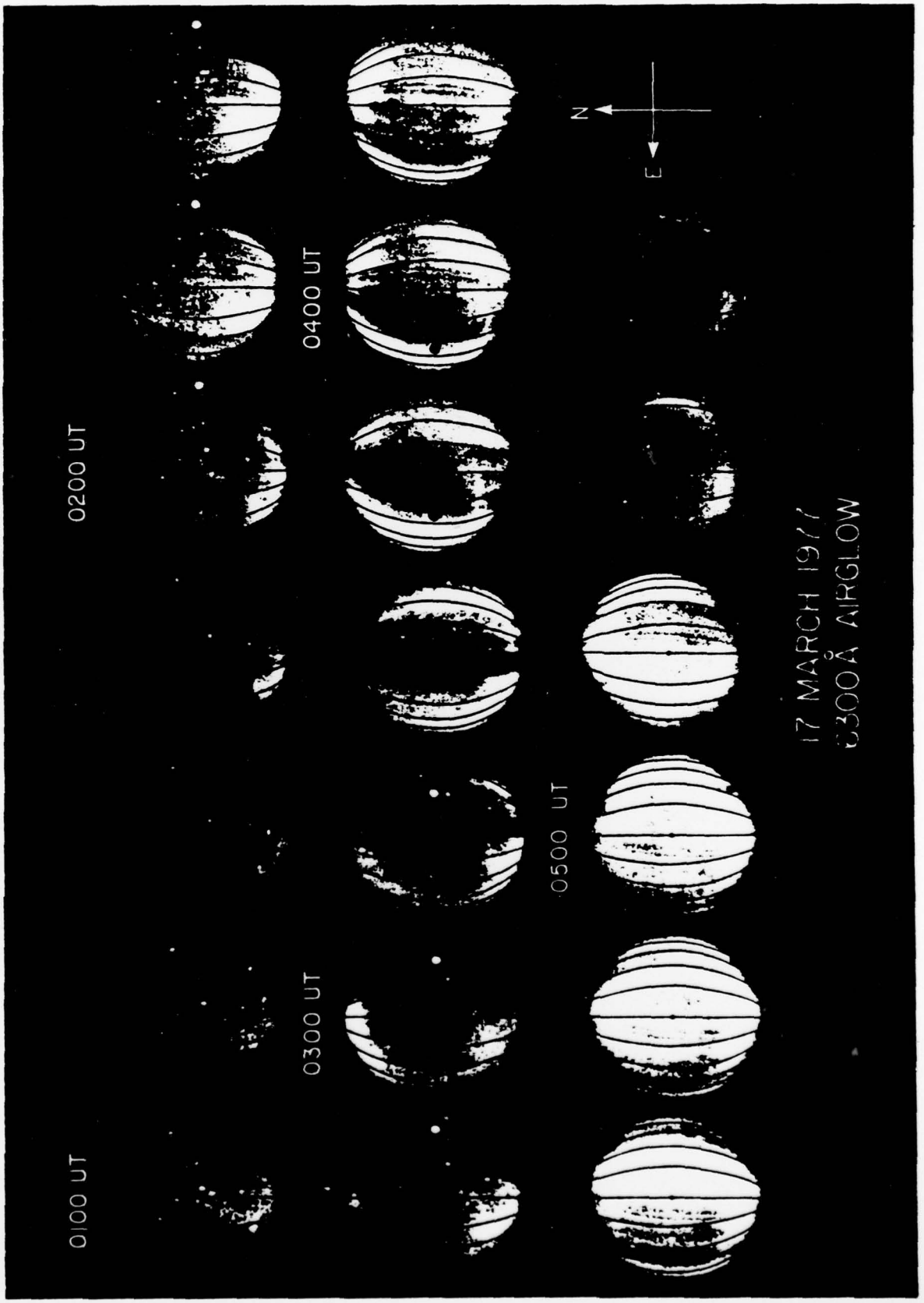
0100 UT
0200 UT
0300 UT
0400 UT
0500 UT
N
E
17 MARCH 1977
6300Å AIRGLOW

FIGURE 1

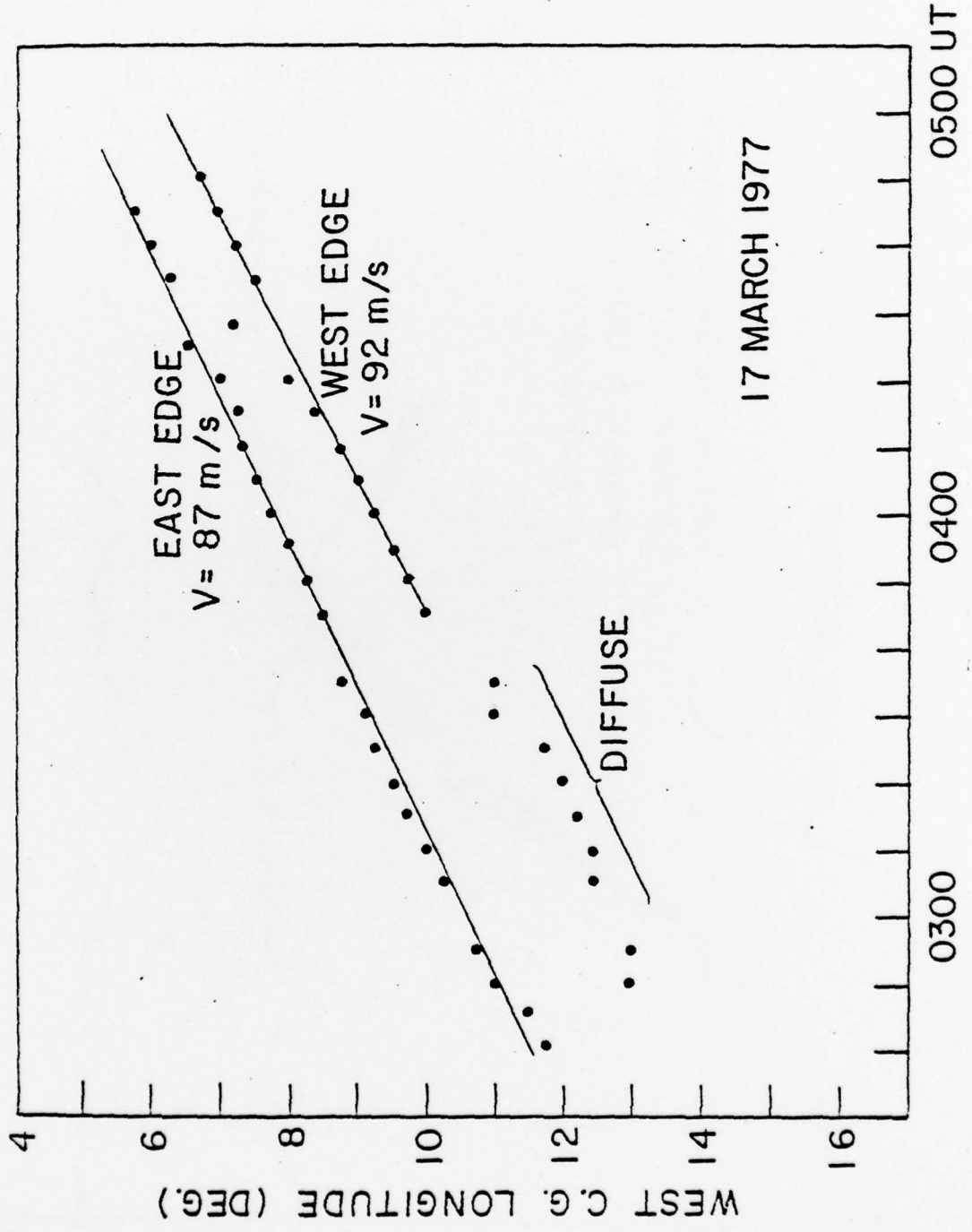
EAST EDGE
V= 87 m/s
WEST EDGE
V= 92 m/s
DIFFUSE
17 MARCH 1977
0300
0400
0500 UT
4
6
8
10
12
14
16
WEST C.G. LONGITUDE (DEG.)

FIGURE 2

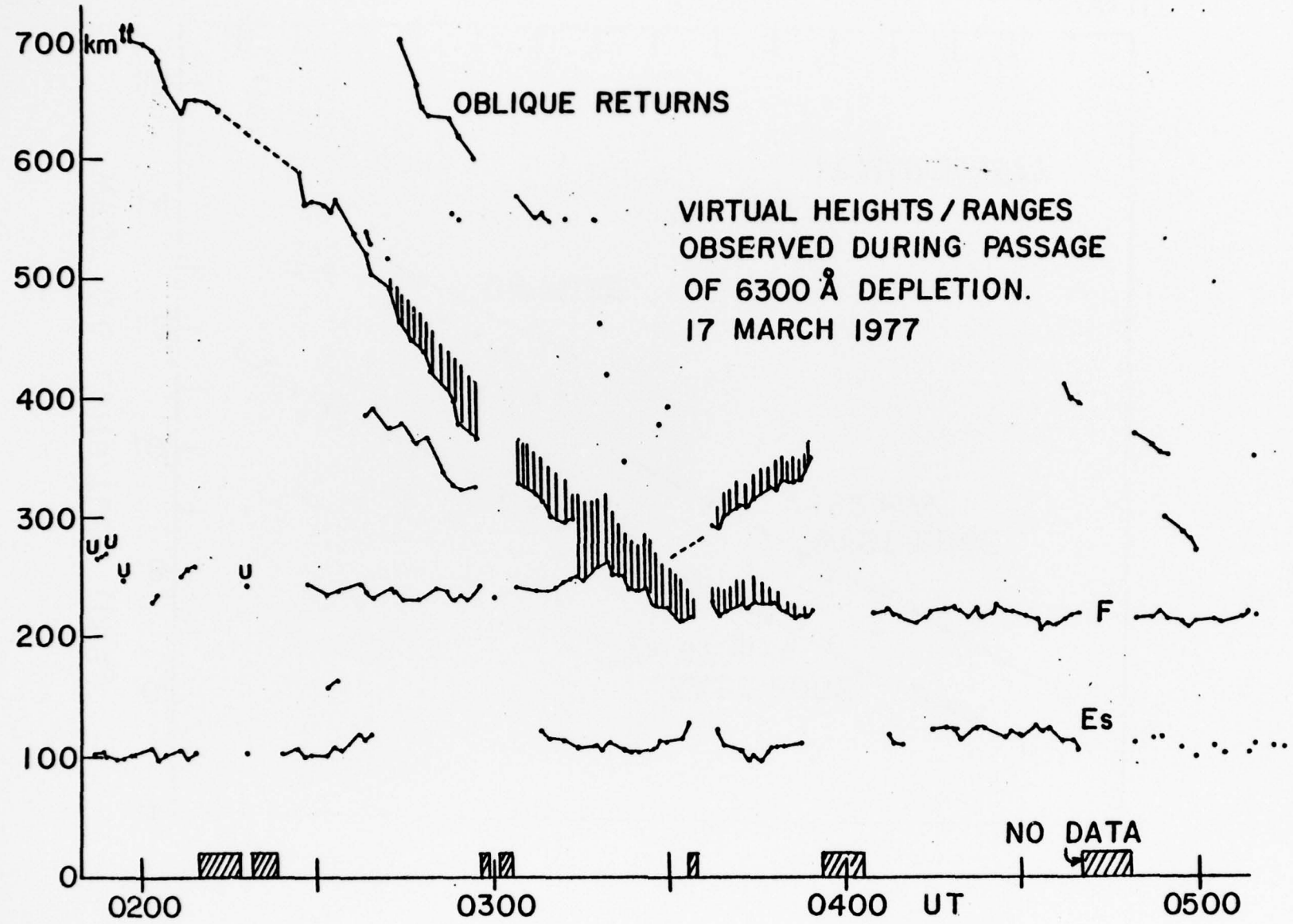
700 km
600
500
400
300
200
100
0
OBLIQUE RETURNS
VIRTUAL HEIGHTS / RANGES
OBSERVED DURING PASSAGE
OF 6300 Å DEPLETION.
17 MARCH 1977
F
Es
NO DATA
0200
0300
0400
UT
0500

FIGURE 3

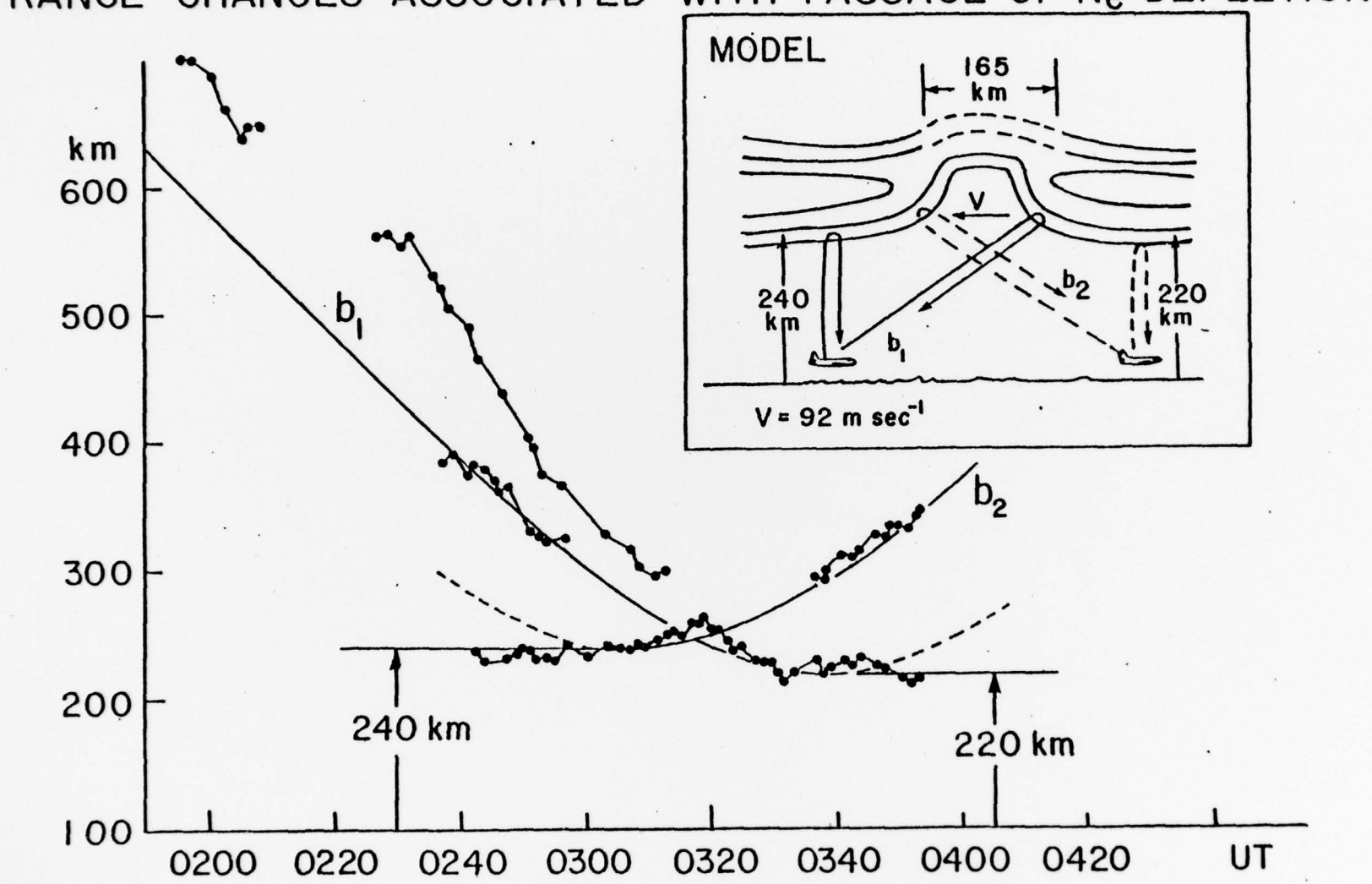
RANGE CHANGES ASSOCIATED WITH PASSAGE OF N_e DEPLETION
MODEL
165 km
V
240 km
220 km
b_1
b_2
V = 92 m sec^{-1}
km
600
500
400
300
200
100
240 km
220 km
0200
0220
0240
0300
0320
0340
0400
0420
UT

FIGURE 4